

Article

# Synthesis, Electrical Properties and Na<sup>+</sup> Migration Pathways of Na<sub>2</sub>CuP<sub>1.5</sub>As<sub>0.5</sub>O<sub>7</sub>

Ohud S. A. ALQarni <sup>1</sup>, Riadh Marzouki <sup>1,2,3,\*</sup>, Youssef Ben Smida <sup>4</sup>, Majed M. Alghamdi <sup>1</sup>, Maxim Avdeev <sup>5,6</sup>, Radhouane Belhadj Tahar <sup>1</sup> and Mohamed Faouzi Zid <sup>3</sup>

<sup>1</sup> Chemistry Department, College of Science, King Khalid University, Abha 61413, Saudi Arabia; 438800025@kku.edu.sa (O.S.A.A.); mmalghamdi@kku.edu.sa (M.M.A.); rhbalhaj@kku.edu.sa (R.B.T.)

<sup>2</sup> Chemistry Department, Faculty of Sciences of Sfax, University of Sfax, Sfax 3038, Tunisia

<sup>3</sup> Laboratoire de Matériaux, Cristallographie et Thermodynamique Appliquée, Faculté des Sciences de Tunis, Université de Tunis El Manar, El Manar II, Tunis 2092, Tunisia; medfaouzi.zid57@gmail.com

<sup>4</sup> Laboratory of valorization of useful materials, National Center of Materials Sciences Research, Technopole Borj Cedria, BP 73, Soliman 8027, Tunisia; youssef.bensmida@fst.utm.tn

<sup>5</sup> Australian Centre for Neutron Scattering, Australian Nuclear Science and Technology Organisation, Sydney 2234, Australia; Maxim.Avdeev@ansto.gov.au

<sup>6</sup> School of Chemistry, The University of Sydney, Sydney 2006, Australia

\* Correspondence: rmarzouki@kku.edu.sa; Tel.: +96-654-284-3436

Received: 10 February 2020; Accepted: 3 March 2020; Published: 6 March 2020



**Abstract:** A new member of sodium metal diphosphate-diarsenate, Na<sub>2</sub>CuP<sub>1.5</sub>As<sub>0.5</sub>O<sub>7</sub>, was synthesized as polycrystalline powder by a solid-state route. X-ray diffraction followed by Rietveld refinement show that the studied material, isostructural with β-Na<sub>2</sub>CuP<sub>2</sub>O<sub>7</sub>, crystallizes in the monoclinic system of the C2/c space group with the unit cell parameters a = 14.798(2) Å; b = 5.729(3) Å; c = 8.075(2) Å; β = 115.00(3)°. The structure of the studied material is formed by Cu<sub>2</sub>P<sub>4</sub>O<sub>15</sub> groups connected via oxygen atoms that results in infinite chains, wavy saw-toothed along the [001] direction, with Na<sup>+</sup> ions located in the inter-chain space. Thermal study using DSC analysis shows that the studied material is stable up to the melting point at 688 °C. The electrical investigation, using impedance spectroscopy in the 260–380 °C temperature range, shows that the Na<sub>2</sub>CuP<sub>1.5</sub>As<sub>0.5</sub>O<sub>7</sub> compound is a fast-ion conductor with σ<sub>350</sub> °C = 2.28 × 10<sup>−5</sup> Scm<sup>−1</sup> and E<sub>a</sub> = 0.6 eV. Na<sup>+</sup> ions pathways simulation using bond-valence site energy (BVSE) supports the fast three-dimensional mobility of the sodium cations in the inter-chain space.

**Keywords:** diphosphate-diarsenate; crystal structure; electrical properties; transport pathways simulation

## 1. Introduction

The research exploration of new inorganic materials with open framework constructed of polyhedra sharing faces, edges and/or corners forming 1D channels, 2D inter-layer spaces or 3D networks where cations are located, is currently an area of intense activity including several disciplines, in particular solid-state chemistry. In particular, alkali metal phosphates were found to have various applications because of their electric, piezoelectric, ferroelectric, magnetic, and catalytic properties [1–4]. Among those, the families of materials with the melilite structure [5], the olivine structure [6] and the sodium super ionic conductor (NaSICON) structure [7], attracted attention for their ionic conduction and exchange of ions [6,7].

More recently, in a series of studies arsenate analogs have been synthesized [8–10]. But, until today phosphate compounds are more studied as cathodes [11,12] compared to arsenate and this is perhaps due to the toxicity of arsenic III (As<sub>2</sub>O<sub>3</sub>). However, the oxide of arsenic V (As<sub>2</sub>O<sub>5</sub>) is less toxic. In addition, the introduction of arsenic into a structure changes its physical and chemical properties

and even toxicity. On the other hand, the comparison of the electrochemical properties of  $\text{LiCoPO}_4$  and  $\text{LiCoAsO}_4$  both with olivine structure and close unit cell parameters, shows reversible (de)intercalation from/into material at average voltages of 4.8 and 4.6 V, respectively for  $\text{LiCoAsO}_4$  [10] and a voltage average of 2.5–5 V for  $\text{LiCoPO}_4$  [11].

The  $\text{Na}_2\text{MP}_2\text{O}_7$  systems ( $M =$  transition metal) [13,14] have a layered structure with the layers  $[\text{MP}_2\text{O}_7]_n^{2n-}$  and the sodium cations localized in the interlayer space, which favors high ionic conductivity. We recently investigated the effect of the substitution of P by As with a larger ionic radius for ionic conductivity and showed the improvement of ionic conductivity for  $\text{Na}_2\text{CoP}_{1.5}\text{As}_{0.5}\text{O}_7$  [15], which has an electrical conductivity value of  $\sigma_{240\text{ }^\circ\text{C}} = 7.91 \times 10^{-5} \text{ Scm}^{-1}$  and an activation energy  $E_a = 0.56 \text{ eV}$  compared to  $\text{Na}_2\text{CoP}_2\text{O}_7$  ( $\sigma_{300\text{ }^\circ\text{C}} = 2 \times 10^{-5} \text{ Scm}^{-1}$ ;  $E_a = 0.63 \text{ eV}$ ) [13].

In our search for new polyanion oxides of sodium and transition metals, the exploration of the  $\text{Na}_2\text{O-CuO-P}_2\text{O}_5\text{-As}_2\text{O}_5$  crystallographic systems allowed us to isolate a new member of di-phosphate arsenates,  $\text{Na}_2\text{CuP}_{1.5}\text{As}_{0.5}\text{O}_7$ , in the polycrystalline powder form. In this paper, characterizations and physicochemical studies of the new member of sodium copper diphosphate-diarsenate material,  $\text{Na}_2\text{CuP}_{1.5}\text{As}_{0.5}\text{O}_7$ , and a comparison with other previous works encountered in the literature will be presented.

## 2. Materials and Methods

A mixture of  $\text{Cu}(\text{NO}_3)_2 \cdot 2.5\text{H}_2\text{O}$ ,  $\text{NH}_4\text{H}_2\text{PO}_4$  and  $\text{Na}_2\text{HAsO}_4 \cdot 7\text{H}_2\text{O}$  in the molar ratio Na:Cu:P:As equal to 2:1:1.5:0.5 was placed in a porcelain crucible and heated to  $350\text{ }^\circ\text{C}$  for 24 h to eliminate the volatile products  $\text{H}_2\text{O}$ ,  $\text{NO}_2$ , and  $\text{NH}_3$ . The obtained powder was ground manually using agate mortar and shaped as cylindrical pellets by a uniaxial press. The obtained pellets were heated to  $600\text{ }^\circ\text{C}$ . After 72 h, the sample was cooled slowly at a rate of  $10\text{ }^\circ\text{C/h}$  down to room temperature. After grinding finely, a blue polycrystalline powder was obtained.

X-ray powder diffraction (XRD) was used to control and ensure the purity of the obtained powder. The analysis was carried out using XRD-6000 (Shimadzu, Japan) with graphite monochromator ( $\text{CuK}\alpha$ ,  $\lambda = 0.154178 \text{ nm}$ ) and a scan range of  $2\theta = 10^\circ\text{--}70^\circ$  with step of about  $0.02^\circ$ . The structure was refined using the Rietveld method by the means of the GSAS computer program [16] (EXPGUI, Gaithersburg, Maryland, USA). The crystallographic data of  $\text{Na}_2\text{CuP}_2\text{O}_7$  [17] was used as a starting set. The obtained structural model was confirmed by the Charge Distribution CHARDI model of validation. The CHARDI calculation was done by using the CHARDI2015 computer program (Nespolo, IUCR) [18].

FTIR spectrometer (Agilent Technologies Cary 630 model) was used to allow a direct indexation of the peaks on a spectral range in wave numbers ranging from ( $1300\text{--}400 \text{ cm}^{-1}$ ).

Differential scanning calorimetry (DSC), with the SDT Q600 model, was used to study the thermal behavior of the obtained and prepared sample. In fact, the device contains two crucibles, one as a reference and the other contains the sample to be analyzed. These two crucibles are heated to  $750\text{ }^\circ\text{C}$  at a rate of  $10\text{ }^\circ\text{C/min}$ . The thermal analysis was carried out under a nitrogen atmosphere to avoid the reaction of the sample with the oxygen in the air.

Energy-dispersive X-ray spectroscopy (EDX) and scanning electron microscopy (SEM, Thermo Fisher Scientific model), were used to identify the present elements and the microstructure of the studied material, respectively.

The electrical measurements were preceded by pretreatment of the sample in order to densify the measured sample by reducing the mean particle size of the synthesized powder. Mechanical grinding for 100 min was carried out using the FRISCH planetary micromill pulverisette 7. The polycrystalline sample was shaped as a cylindrical pellet using a uniaxial press. The pellet was sintered in air at an optimal temperature of  $610\text{ }^\circ\text{C}$  for 2 h with  $5\text{ }^\circ\text{C/min}$  heating and cooling rates. The geometric factor of the dense ceramic is  $g = e/S = 0.793 \text{ cm}^{-1}$  where  $e$  and  $S$  are the thickness and face area of pellet, respectively. Gold metal electrodes  $\sim 36 \text{ nm}$  thick were deposited using a SC7620 mini sputter coater.

The sample was then placed between two platinum electrodes that were connected by platinum cables to the frequency response analyzer (HP 4192A) which was controlled by a microcomputer.

Impedance spectroscopic measurements were performed via the Hewlett-Packard 4192-A automatic bridge supervised by HP workstation. Impedance spectra were recorded with 0.5 V AC-signal in the 5 Hz–13 MHz frequency range.

The bond-valence site energy (BVSE) model [19,20] was used to simulate the alkali migration in the 3D anionic framework. The BVSE model is the latest extension of the bond-valence sum (BVS) model developed by Pauling [21] to describe the formation of inorganic materials. The BVS model was improved by Brown & Altermatt [22] followed by Adams [23], resulting in the expression:

$$s_{A-X} = \exp\left(\frac{R_0 - R_{A-X}}{b}\right) \quad (1)$$

where  $s_{A-X}$  is individual bond-valence,  $R_{A-X}$  is the distance between counter-ions A and X,  $R_0$  and  $b$  are fitted empirical constants, and  $R_0$  is the length of a bond of unit valence.

The BVSE model was extensively used in the cation motion simulation in the anionic framework by following the valence unit as a function of migration distance [24]. The valence unit was also recently related to potential energy scale and electrostatic interactions [19,20]. The BVSE method was used with success to simulate the transport pathways of monovalent cations ( $\text{Na}^+$ ;  $\text{K}^+$  and  $\text{Ag}^+$ ) in numerous materials including  $\text{Na}_2\text{CoP}_{1.5}\text{As}_{0.5}\text{O}_7$  [15],  $\text{Na}_{1.14}\text{K}_{0.86}\text{CoP}_2\text{O}_7$  [25] and  $\text{Ag}_{3.68}\text{Co}_2(\text{P}_2\text{O}_7)_2$  [26]. The BVSE calculations were performed using the SoftBV [27] code and the visualization of isosurfaces was carried out using VESTA3 software (version 3, Koichi Momma and Fujio Izumi, 2018).

### 3. Results and Discussion

#### 3.1. X-ray Powder Diffraction

The crystallographic study was started by a simple comparison between the XRD pattern of the prepared materials in the  $\text{Na}_2\text{O-CuO-P}_2\text{O}_5\text{-As}_2\text{O}_5$  system and those of the previous studies of diphosphate  $\text{Na}_2\text{MP}_2\text{O}_7$  [5,7,14,28,29] and  $\text{Na}_2\text{CoP}_{1.5}\text{As}_{0.5}\text{O}_7$  [15]. In this case, only the  $\text{Na}_2\text{CuP}_{1.5}\text{As}_{0.5}\text{O}_7$  diffractogram showed a similarity with that of the  $\beta\text{-Na}_2\text{CuP}_2\text{O}_7$  diphosphate [17]. It crystallizes in the monoclinic system of the C2/c space group. This result prompted us to make a precise refinement using the Rietveld method which was implemented into the GSAS computer software [16]. The final agreement factors are  $R_p = 5.4\%$  and  $R_{wp} = 6.9\%$ . No additional peaks were detected. The final Rietveld plot is presented in Figure 1. The unit cell parameters obtained from the Rietveld refinement are  $a = 14.798(2)$  Å;  $b = 5.729(3)$  Å;  $c = 8.075(2)$  Å;  $\beta = 115.00(3)^\circ$  (Table 1). The details of the crystallographic data, data collection and final agreement factors are given in Table 2. The atomic coordinates and isotropic displacement parameters are listed in Table 3. The main bond distances are given in Table 4. The charge distribution analysis and the bond-valence computation are summarized in Table 5.

**Table 1.** Unit cell parameters of the  $\beta\text{-Na}_2\text{CuP}_2\text{O}_7$  and  $\text{Na}_2\text{CuP}_{1.5}\text{As}_{0.5}\text{O}_7$  materials.

Parameter	$\text{Na}_2\text{CuP}_{1.5}\text{As}_{0.5}\text{O}_7$ (Current Work)	$\beta\text{-Na}_2\text{CuP}_2\text{O}_7$ [30]
$a$ (Å)	14.798(2)	14.728(3)
$b$ (Å)	5.729(3)	5.698(1)
$c$ (Å)	8.075(2)	8.067(1)
$\beta$ (°)	115.00(3)	115.15(1)
$V$ (Å <sup>3</sup> )	620.43(3)	612.80(2)

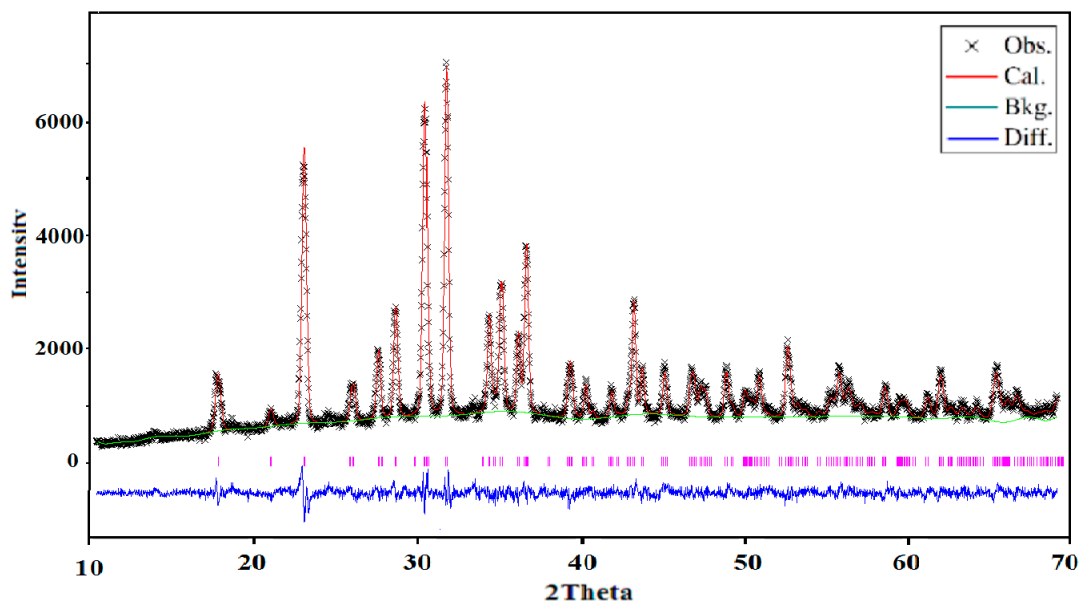


Figure 1. Results of the Rietveld refinement of the powder of  $\text{Na}_2\text{CuP}_{1.5}\text{As}_{0.5}\text{O}_7$  based on XRD data.

Table 2. Structure refinement results of the  $\text{Na}_2\text{CuP}_{1.5}\text{As}_{0.5}\text{O}_7$  compound.

Crystallographic Data	
Empirical Formula	$\text{Na}_2\text{CuP}_{1.5}\text{As}_{0.5}\text{O}_7$
Formula Weight; $\rho_{\text{cal}}$	305.44 g mol <sup>-1</sup> ; 3.220 g cm <sup>-3</sup>
Crystalline System; Space Group	Monoclinic, C2/c
Unit Cell Dimensions	a = 14.8688 (8), b = 5.7591 (3), c = 13.5957 (7) $\beta$ = 147.2406 (12)
Volume; Z	V = 629.97 (6) $\text{\AA}^3$ ; 4
Data Collection	
Diffractometer	Bruker D8 ADVANCE
Wavelength	$\lambda_{\text{Cu K}\alpha} = 1.54056 \text{ \AA}$
Temperature	298 (2) K
Angle Range	4.91°–69.91°
Step Scan Increment (°2 $\theta$ )	0.02°
Counting Time	2 s
Refinement	
Angle Range	4.91°–69.91°
$R_p$	0.054
$R_{wp}$	0.069
$R_{exp}$	0.043
$R(F^2)$	0.05117
Goodness of Fit $\chi^2$	2.592
No. of Data Points	3251
No. of Restraints	18
Profile Function	Pseudo-Voigt
Background	Chebyshev function with 20 terms

**Table 3.** Fractional atomic coordinates and equivalent isotropic displacement parameters ( $\text{\AA}^2$ ).

	x	y	z	$U_{\text{iso}}$	Occ. (<1)
Cu1	$\frac{1}{4}$	$\frac{1}{4}$	$\frac{1}{2}$	0.0123 (12)	
P1/As1	0.5112 (2)	0.5884 (5)	0.6563 (3)	0.0065 (14)	0.75/0.25
Na1	0.3211 (5)	0.8919 (9)	0.2991 (5)	0.004 (2)	
O1	0.6590 (6)	0.4179 (9)	0.7999 (6)	0.006 (2)	
O2	0.5389 (4)	0.7622 (10)	0.6011 (6)	0.006 (2)	
O3	0.8432 (6)	0.0371 (12)	0.9916 (5)	0.041 (5)	
O4	$\frac{1}{2}$	0.7267 (9)	$\frac{3}{4}$	0.018 (5)	

**Table 4.** Main bond distances ( $\text{\AA}$ ) in the coordination polyhedra for  $\text{Na}_2\text{CuP}_{1.5}\text{As}_{0.5}\text{O}_7$ .

$\text{Cu1O}_4$		$(\text{P1/As1})\text{O}_4$	
Cu1—O1 <sup>iii</sup>	1.9938 (3)	(P1/As1)—O1	1.5457 (3)
Cu1—O1 <sup>x</sup>	1.9938 (3)	(P1/As1)—O2	1.5015 (3)
Cu1—O3 <sup>iii</sup>	1.9247 (3)	(P1/As1)—O3 <sup>x</sup>	1.5387 (3)
Cu1—O3 <sup>x</sup>	1.9247 (3)	(P1/As1)—O4	1.6248 (3)
Na1O <sub>6</sub>			
Na1—O1 <sup>i</sup>	2.3985 (4)	Na1—O2 <sup>iv</sup>	2.3220 (4)
Na1—O1 <sup>vi</sup>	2.6566 (4)	Na1—O2 <sup>vi</sup>	2.5780 (4)
Na1—O2	2.3541 (4)	Na1—O3 <sup>i</sup>	2.3485 (4)

Symmetry codes: (i)  $-x + 1, -y + 1, -z + 1$ ; (ii)  $x - 1/2, -y + 1/2, z + 1/2$ ; (iii)  $-x + 1, y, -z + 3/2$ ; (iv)  $-x + 1, -y + 2, -z + 1$ ; (v)  $x - 1/2, -y - 1/2, z + 1/2$ ; (vi)  $x - 3/2, -y + 1/2, z - 1/2$ ; (vii)  $-x + 1/2, y - 1/2, -z + 1/2$ ; (viii)  $-x + 1/2, y + 1/2, -z + 1/2$ ; (ix)  $x, -y + 1, z - 1/2$ ; (x)  $x - 3/2, -y - 1/2, z - 1$ .

**Table 5.** Charge distribution analysis of cation polyhedra in  $\text{Na}_2\text{CuP}_{1.5}\text{As}_{0.5}\text{O}_7$ .

Cation	q(i).sof(i)	Q(i)	CN(i)	ECoN(i)	$d_{\text{ar}}(i)$	$d_{\text{med}}(i)$
Cu1	2.000	1.96	4	3.96	1.955	1.959
M1	5.000	5.03	4	3.88	1.544	1.552
Na1	1.000	0.98	6	5.47	2.400	2.443

q(i), formal oxidation number; Q(i), computed charge; sof(i), site occupation factor;  $d_{\text{ar}}(i)$ , arithmetic average distance;  $d_{\text{med}}(i)$ , weighted average distance; CN, coordination number; ECoN(i), effective coordination number. M1 = (0.75P + 0.25As=).

By comparing the unit cell parameters of the studied material with those of  $\beta\text{-Na}_2\text{CuP}_2\text{O}_7$ , the P/As substitution effect increases the volume of the unit cell (Table 1), which is explained by the distance of As—O bonds being greater than that of P—O.

### 3.2. Infrared Spectroscopy

The IR absorption spectrum of the studied  $\text{Na}_2\text{CuP}_{1.5}\text{As}_{0.5}\text{O}_7$  material is shown in Figure 2. The spectrum shows the presence of the series of distinct bands attributed to asymmetric and symmetrical valence vibrations of the P-O-P and As-O-As bridges. These bands are characteristic of the pyrophosphate ( $\text{P}_2\text{O}_7$ )<sup>4-</sup> and diarsenate ( $\text{As}_2\text{O}_7$ )<sup>4-</sup> groups (Table 6) [30] and similar to those of the  $\text{Li}_2\text{CuP}_2\text{O}_7$  spectrum [31].

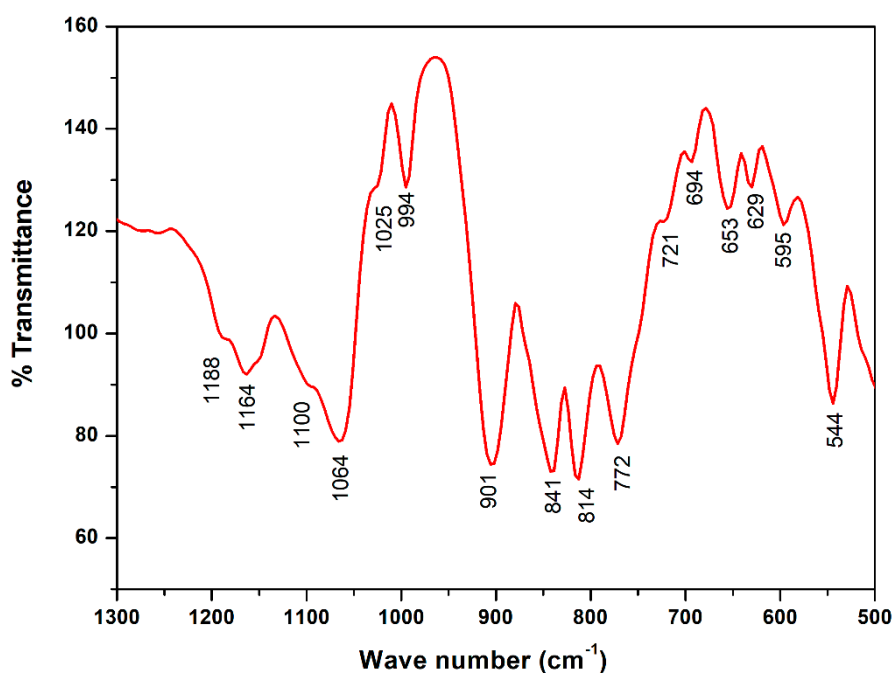


Figure 2. FT-IR spectrum (1300–500  $\text{cm}^{-1}$ ) of  $\text{Na}_2\text{CuP}_{1.5}\text{As}_{0.5}\text{O}_7$ .

Table 6. Proposed assignment of the vibration bands of  $\text{Na}_2\text{CuP}_{1.5}\text{As}_{0.5}\text{O}_7$ .

Attribution	Wave Number ( $\text{cm}^{-1}$ )
$\nu_{\text{as}}$ ( $\text{PO}_3$ )	1188
	1164
$\nu_{\text{as}}$ ( $\text{AsO}_3$ )	1100
$\nu_{\text{s}}$ ( $\text{PO}_3$ )	1064
	1025
$\nu_{\text{s}}$ ( $\text{AsO}_3$ )	994
$\nu_{\text{as}}$ (POP) Stretching Vibrations	901
$\nu_{\text{as}}$ (AsOAs) Stretching Vibrations	841
	814
$\nu_{\text{s}}$ (POP) Stretching Vibrations	772
	721
$\nu_{\text{s}}$ (AsOAs) Stretching Vibrations	694
	653
	629
$\delta_{\text{as}}$ ( $\text{PO}_3$ ) Deformation Modes	595
	544

### 3.3. DSC Thermal Analysis

In order to determine the thermal stability of the studied compound, the DSC analysis was used in the range from room temperature to 750  $^{\circ}\text{C}$ . The analysis result is illustrated in Figure 3. An endothermic peak was observed at 688  $^{\circ}\text{C}$ . This peak corresponds to the melting point of our compound. While, an exothermic peak is shown at 743  $^{\circ}\text{C}$ , after the fusion, probably corresponds to the oxidation of fractions of  $\text{Cu}^{2+}$  to  $\text{Cu}^{3+}$  in the obtained liquid phase. Overall, the thermal analysis

via DSC shows that  $\text{Na}_2\text{CuP}_{1.5}\text{As}_{0.5}\text{O}_7$  material is stable up to a temperature of  $674^\circ\text{C}$ . The sharpness of the endothermic peak in the DSC analysis suggests good crystallinity of our synthesized powder.

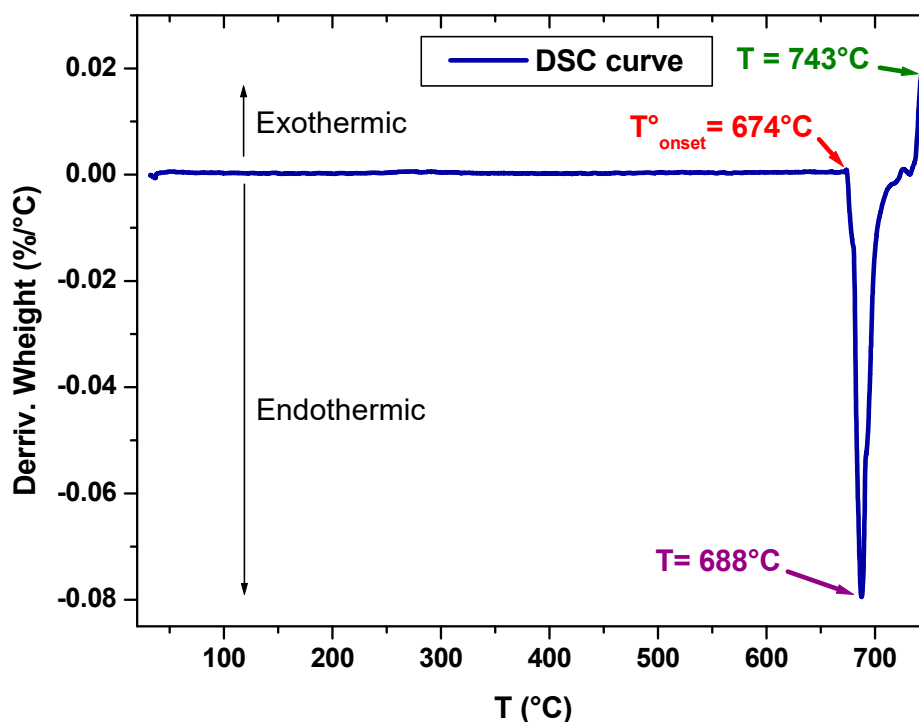


Figure 3. DSC curve of the  $\text{Na}_2\text{CuP}_{1.5}\text{As}_{0.5}\text{O}_7$  compound.

Here we can also compare the thermal stability of  $\text{Na}_2\text{CuP}_{1.5}\text{As}_{0.5}\text{O}_7$  to that of the recently studied Co analog  $\text{Na}_2\text{CoP}_{1.5}\text{As}_{0.5}\text{O}_7$ . The Cu material is stable from room temperature to the melting temperature, which is around  $688^\circ\text{C}$ . In contrast, the  $\text{Na}_2\text{CoP}_{1.5}\text{As}_{0.5}\text{O}_7$  material undergoes a phase transition at a temperature of  $675^\circ\text{C}$  before melting at  $\sim 700^\circ\text{C}$ . This shows that the  $\text{Na}_2\text{CuP}_{1.5}\text{As}_{0.5}\text{O}_7$  material is more stable than the  $\text{Na}_2\text{CoP}_{1.5}\text{As}_{0.5}\text{O}_7$  material [15].

#### 3.4. SEM Microstructure and EDX Analysis of $\text{Na}_2\text{CuP}_{1.5}\text{As}_{0.5}\text{O}_7$

Energy-dispersive X-ray spectroscopy (EDX) and scanning electron microscopy (SEM) analysis were used to confirm the chemical composition and examine polycrystalline morphology, respectively (Figure 4). The EDX analysis of the polycrystalline powder revealed the presence of the expected elements, i.e., sodium, copper, phosphorus, arsenic, and oxygen. The micrograph on SEM of the sample shows agglomeration of uniform parallelepiped crystallites. The mapping elemental analysis of  $\text{Na}_2\text{CuP}_{1.5}\text{As}_{0.5}\text{O}_7$  confirmed the uniform distribution of the constituent elements (Figure 5).

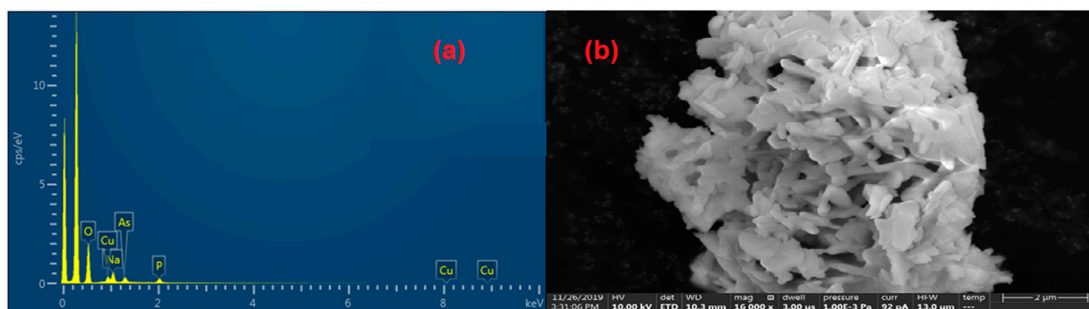
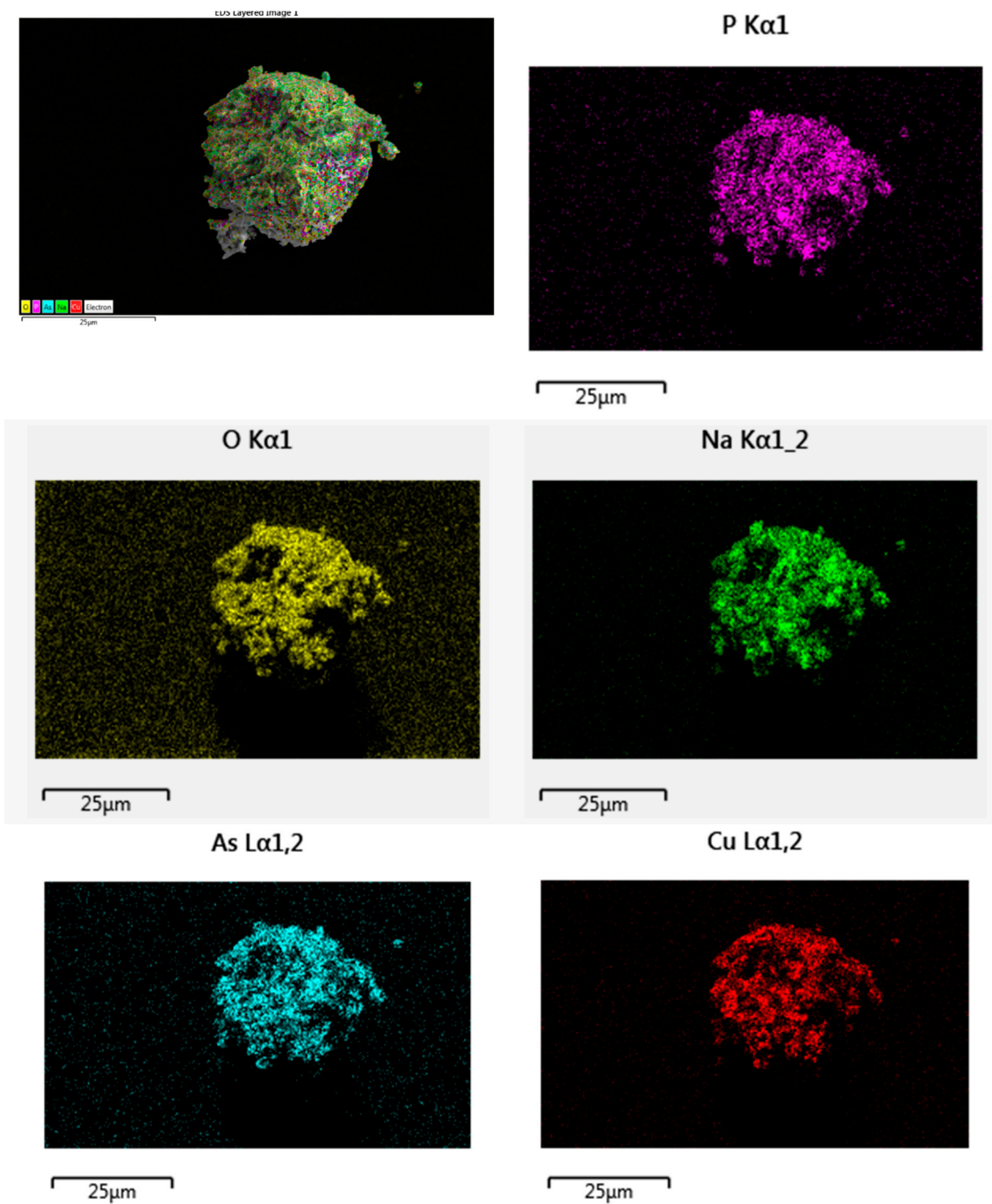


Figure 4. (a) EDX analysis and (b) SEM micrograph of the  $\text{Na}_2\text{CuP}_{1.5}\text{As}_{0.5}\text{O}_7$  sample.



**Figure 5.** The mapping elemental analysis of the  $\text{Na}_2\text{CuP}_{1.5}\text{As}_{0.5}\text{O}_7$  sample.

### 3.5. Crystal Structure Description

The structural unit of  $\text{Na}_2\text{CuP}_{1.5}\text{As}_{0.5}\text{O}_7$  is presented in Figure 6. It contains two  $\text{P}_2\text{O}_7$  units connected by a vertex with two  $\text{CuO}_4$  of square planar geometry. The charge neutrality of the structural unit is ensured by four sodium ions ( $\text{Na}^+$ ).

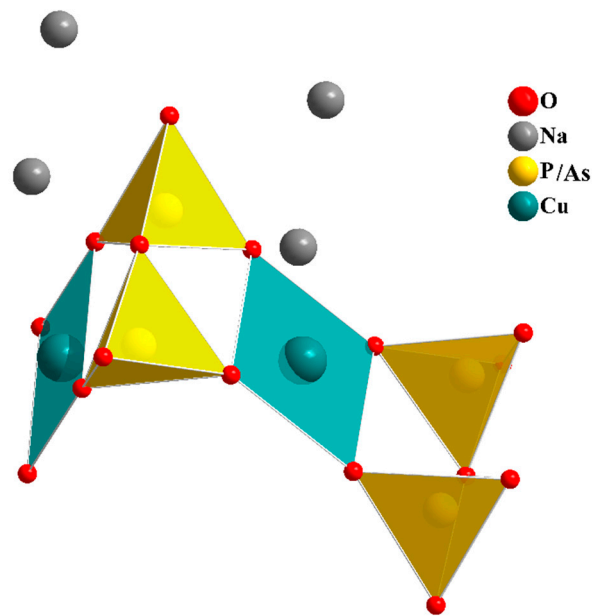


**Figure 6.** The structural unit of  $\text{Na}_2\text{CuP}_{1.5}\text{As}_{0.5}\text{O}_7$ .

The  $\text{Cu}_2\text{P}_4\text{O}_{15}$  groups of the structural unit are bound by oxygen peaks to result in infinite chains and are wavy saw-toothed along the  $[001]$  direction (Figure 7). The  $\text{Na}^+$  ions are located in the inter-chain space.

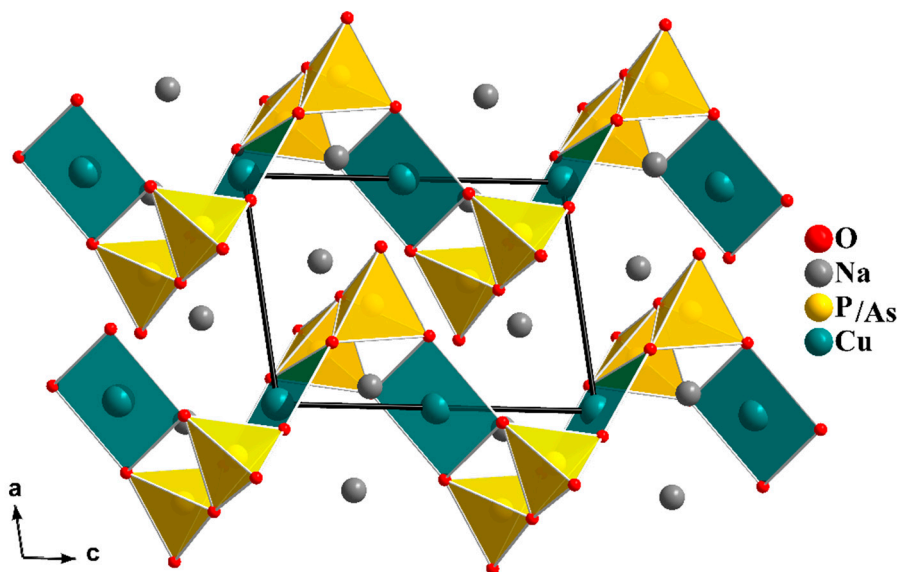


**Figure 7.** View of the structure of  $\text{Na}_2\text{CuP}_{1.5}\text{As}_{0.5}\text{O}_7$  in the  $ac$  plane showing the arrangement of the chains.

Other projections of the structure of  $\text{Na}_2\text{CuP}_{1.5}\text{As}_{0.5}\text{O}_7$  according to the  $[100]$  and  $[001]$  directions are shown in Figure 8.

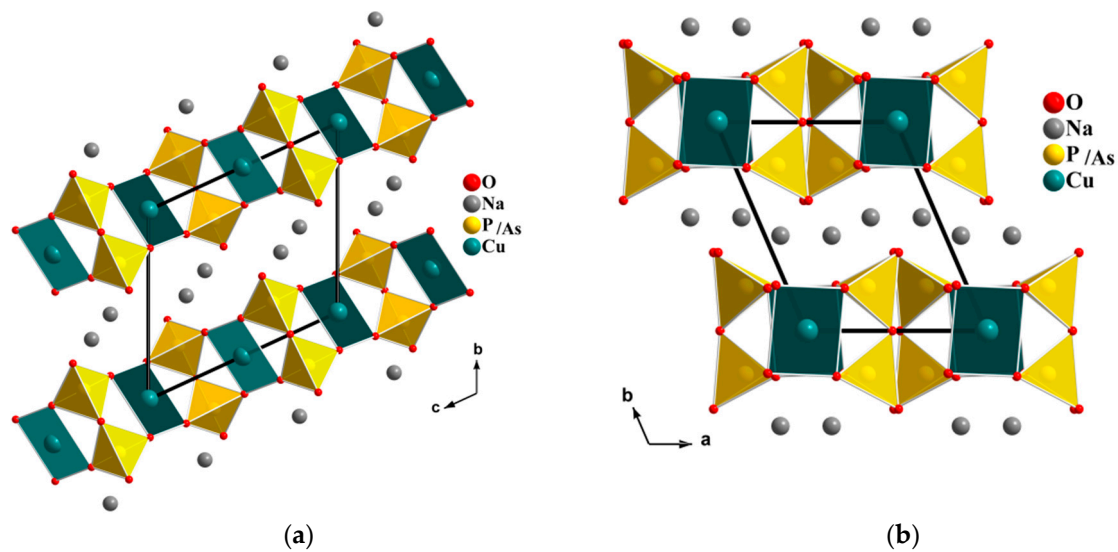


**Figure 8.** Projections of the  $\text{Na}_2\text{CuP}_{1.5}\text{As}_{0.5}\text{O}_7$  structure along the (a) [100] and (b) [001] directions.

The structure of our material differs from that of the allotropic form  $\alpha\text{-Na}_2\text{CuP}_2\text{O}_7$  [17], which has a two-dimensional anionic framework formed by the connection of vertices of  $\text{PO}_4$  tetrahedra, and  $\text{CuO}_5$  polyhedra.

Compared to the sodium cobalt diphosphate-diarsenate  $\text{Na}_2\text{CoP}_{1.5}\text{As}_{0.5}\text{O}_7$  investigated recently by Marzouki et al. [15], we notice that despite a similar composition,  $\text{Na}_2\text{CuP}_{1.5}\text{As}_{0.5}\text{O}_7$  crystallizes in a different structure type. Indeed, the cobalt material crystallizes in the tetragonal system of the  $\text{P4}_2/\text{mmn}$  space group with the unit cell parameters  $a = 7.764(3) \text{ \AA}$ ,  $c = 10.385(3) \text{ \AA}$ . In contrast, the studied material  $\text{Na}_2\text{CuP}_{1.5}\text{As}_{0.5}\text{O}_7$ , crystallizes in the monoclinic system of the  $\text{C2}/c$  space group with the unit cell parameters  $a = 14.798(2) \text{ \AA}$ ;  $b = 5.729(3) \text{ \AA}$ ;  $c = 8.075(2) \text{ \AA}$ ;  $\beta = 115.00(3)^\circ$ . The difference is undoubtedly determined by the preference of the Jahn–Teller active  $d^9 \text{Cu}^{2+}$  to adopt square coordination (Figure 6).

### 3.6. Electrical Properties: Effect of P/As Doping

The prepared pellet of the  $\text{Na}_2\text{CuP}_{1.5}\text{As}_{0.5}\text{O}_7$  compound was sintered at  $550 \text{ }^\circ\text{C}$  for 2 h with a  $5 \text{ }^\circ\text{C}/\text{min}$  heating and cooling rate. The relative density of the obtained pellet is  $D = 88\%$ . The thickness and surface of the pellet are  $e = 0.36 \text{ cm}$  and  $S = 0.454 \text{ cm}^2$ , respectively. The electrical measurements of the obtained sample were carried out using complex impedance spectroscopy in the temperature range of  $260\text{--}380 \text{ }^\circ\text{C}$ . The recorded spectra are shown in Figure 9.

The best fits of impedance spectra were obtained when using a conventional electrical circuit  $R_g//\text{CPE}_g\text{-}R_{gb}//\text{CPE}_{gb}$ , where CPE are constant phase elements (Figure 9a) and subscripts g and gb indicate bulk grain and grain boundary contribution, respectively:

$$Z_{\text{CPE}} = \frac{1}{A(j\omega)^p} \quad (2)$$

The true capacitance was calculated from the pseudo-capacitance according to the following relationships:

$$O_0 = (RA)^{-1/p} = (RC)^{-1} \quad (3)$$

(where  $\omega_0$  is the relaxation frequency,  $A$  is the pseudo-capacitance obtained from the CPE, and  $C$  is the true capacitance.

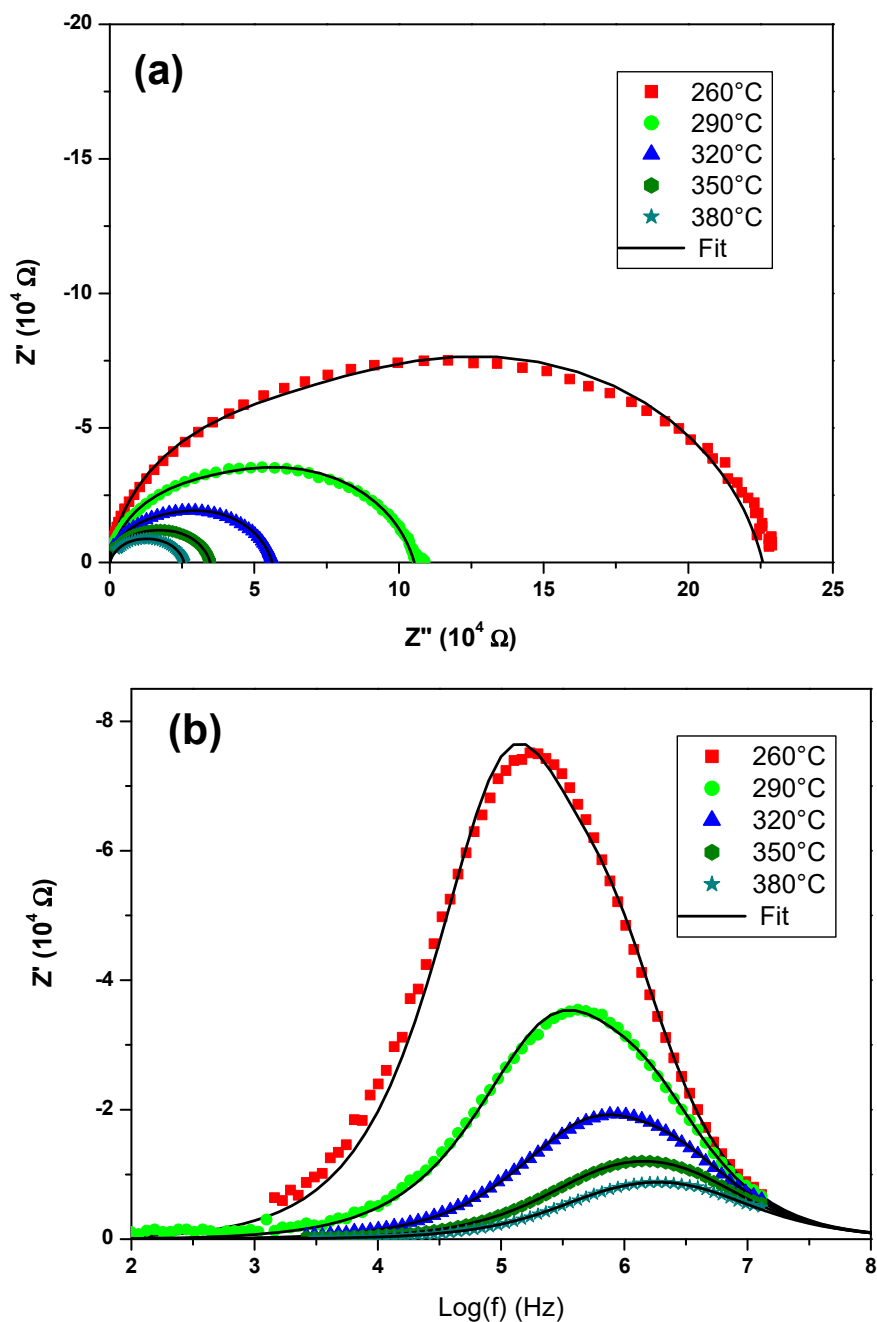


**Figure 9.** Impedance spectra of  $\text{Na}_2\text{CuP}_{1.5}\text{As}_{0.5}\text{O}_7$  recorded in a temperature range of 240–360 °C in air. The refined calculated model is shown in (a) the Nyquist and (b) Bode planes.

The electrical parameter values calculated at different temperatures are shown in Table 4. The values of the capacities  $C_{gk}$  and  $C_{gbk}$  are approximately  $10^{-11}$  and  $10^{-10} \text{ Fcm}^{-1}$  for the bulk and grain boundaries, respectively [15]. In fact, with a relative density of  $D = 88\%$ , the conductivity of the prepared sample (Table 7) increases from  $0.35 \cdot 10^{-5} \text{ Scm}^{-1}$  at 260 °C to  $3.13 \cdot 10^{-5} \text{ Scm}^{-1}$  at 380 °C. On the other hand, the 12% porosity of our sample prompted us to estimate the conductivity values of the fully dense sample of  $\text{Na}_2\text{CuP}_{1.5}\text{As}_{0.5}\text{O}_7$  using the empirical formula proposed by Langlois and Coeuret [32]:

$$\sigma = \frac{(1 - P)}{4} \sigma_d \quad (4)$$

where  $\sigma$  and  $\sigma_d$  are the electrical conductivity of porous and dense samples, respectively.  $P$  is the porosity of the sample.

**Table 7.** Electrical parameters values of equivalent circuits of  $\text{Na}_2\text{CuP}_{1.5}\text{As}_{0.5}\text{O}_7$  determined by impedance spectroscopy at 260–380 °C.

T (°C)	T (K)	$R_g$ ( $10^4 \Omega$ )	$A_g$ ( $10^{-10} \text{ F s}^{\text{P}-1}$ )	$C_{gk}$ ( $10^{-11} \text{ F cm}^{-1}$ )	$R_{gb}$ ( $10^4 \Omega$ )	$A_{gb}$ ( $10^{-10} \text{ F s}^{\text{P}-1}$ )	$C_{gbk}$ ( $10^{-10} \text{ F cm}^{-1}$ )	$R_t$ ( $10^4 \Omega$ )	$\rho_t$ ( $10^4 \Omega \text{ cm}$ )	$\sigma$ ( $10^{-5} \text{ S cm}^{-1}$ )	$\sigma_d$ ( $10^{-5} \text{ S cm}^{-1}$ )
260	533	5.54	2.1	2.0	17.04	1.7	1.7	22.58	28.58	0.35	1.59
290	563	2.70	3.4	3.3	7.82	1.8	1.70	10.52	13.32	0.75	3.41
320	593	1.43	3.4	3.3	4.18	1.5	1.5	5.61	7.10	1.41	6.41
350	623	1.21	3.4	3.3	2.26	1.4	1.3	3.47	4.39	2.28	10.36
380	653	1.01	8.4	8.0	1.51	1.2	1.2	2.52	3.19	3.13	14.23

This correction has been used in previous works such as  $\text{Na}_2\text{CoP}_{1.5}\text{As}_{0.5}\text{O}_7$  [15]. Taking into account the porosity factor  $P = 0.12$ , the conductivity value of dense material will be  $\sigma_d = (4\sigma/0.88)$ . The conductivity values of dense sample calculated at different temperatures are summarized in Table 7. In this case, the experimental conductivity of  $3.5 \times 10^{-6} \text{ Scm}^{-1}$  corresponds to the corrected value of  $1.59 \times 10^{-5} \text{ Scm}^{-1}$  at  $260 \text{ }^\circ\text{C}$ .

The curve  $\text{Ln}(\sigma \times T) = f(1000/T)$  is linear (Figure 10), satisfying the Arrhenius law  $\text{Ln}\sigma T = \text{Ln}\sigma_0 - E_a/kT$  ( $k =$  Boltzmann constant). The activation energy calculated from the slope of this curve is  $E_a = 0.60 \text{ eV}$ .

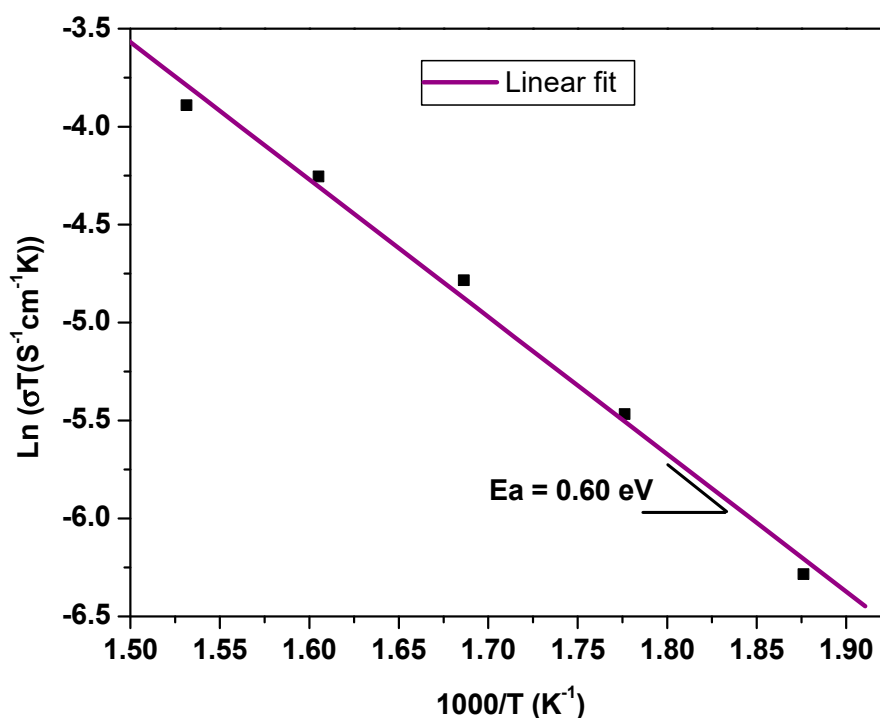


Figure 10. Arrhenius plot of the conductivity of the  $\text{Na}_2\text{CuP}_{1.5}\text{As}_{0.5}\text{O}_7$  sample.

The electrical investigation of the studied material shows that the activation energy, which is unaffected by porosity and thus easier to use for comparison, decreases for  $\text{Na}_2\text{CuP}_{1.5}\text{As}_{0.5}\text{O}_7$  compared to that of  $\text{Na}_2\text{CuP}_2\text{O}_7$  [33], i.e., 0.60 eV and 0.89 eV, respectively. Consequently, the effect of P/As substitution increases the electrical conductivity of the parent material  $\text{Na}_2\text{CuP}_2\text{O}_7$  at lower temperatures [33]. Overall, a comparison of the conductivity values of the studied material  $\text{Na}_2\text{CuP}_{1.5}\text{As}_{0.5}\text{O}_7$  (at  $T = 350 \text{ }^\circ\text{C}$ ,  $\sigma_{D=88\%} = 2.28 \times 10^{-5} \text{ Scm}^{-1}$ ;  $\sigma_d = 2.28 \times 10^{-4} \text{ Scm}^{-1}$  and  $E_a = 0.60 \text{ eV}$ ) with those found in the literature shows that our material can be classified among the fast ionic conductors as shown in Table 8.

Table 8. Activation energies of ionic conductivity for some sodium-ion materials.

Material	Activation Energy (eV)	Temperature Range ( $^\circ\text{C}$ )	Ref.
$\text{Na}_2\text{CuP}_{1.5}\text{As}_{0.5}\text{O}_7$	0.60	260–380	current work
$\text{Na}_2\text{CoP}_{1.5}\text{As}_{0.5}\text{O}_7$	0.56	240–360	[15]
$\text{Na}_{1.14}\text{K}_{0.86}\text{CoP}_2\text{O}_7$	1.34	360–480	[24]
$\text{Na}_{2.84}\text{Ag}_{1.16}\text{Co}_2(\text{P}_2\text{O}_7)_2$	1.36	510–630	[34]
$\text{NaCo}_2\text{As}_3\text{O}_{10}$	0.48	160–410	[35]
$\text{Na}_4\text{Co}_{5.63}\text{Al}_{0.91}(\text{AsO}_4)_6$	0.56	400–550	[36]
$\text{Na}_2\text{Co}_2(\text{MoO}_4)_3$	1.20	180–513	[37]

### 3.7. BVSE Simulation: Na<sup>+</sup> Migration Pathways in Na<sub>2</sub>CuP<sub>1.5</sub>As<sub>0.5</sub>O<sub>7</sub>

The BVSE calculation revealed in addition to the equilibrium site Na1, the presence of two interstitial sites (i1 to i2) and ten saddle points (s1 to s10) (Table 9). Thus, there are ten local pathways as shown in Table 10. Figure 11 shows the position of equilibrium sites and interstitial sites in the unit cell.

**Table 9.** Bond-valence sites energies and positions of equilibrium site (Na1), interstitial sites (i1 and i2) and saddle points (s1 to s10).

Site	x	y	z	Energy (eV)
Na1	0.185	0.611	0.701	0.000
i1	0.524	0.875	0.424	0.288
i2	0.262	0.194	0.986	0.715
s1	0.560	0.125	0.632	0.354
s2	0.226	0.083	0.215	0.466
s3	0.006	0.389	0.250	0.550
s4	0.125	0.528	0.069	0.602
s5	0.250	0.250	0.000	0.749
s6	0.173	0.431	0.958	0.870
s7	0.714	0.208	0.583	0.960
s8	0.821	0.708	0.375	1.260
s9	0.190	0.333	0.653	1.289
s10	0.167	0.361	0.833	1.643

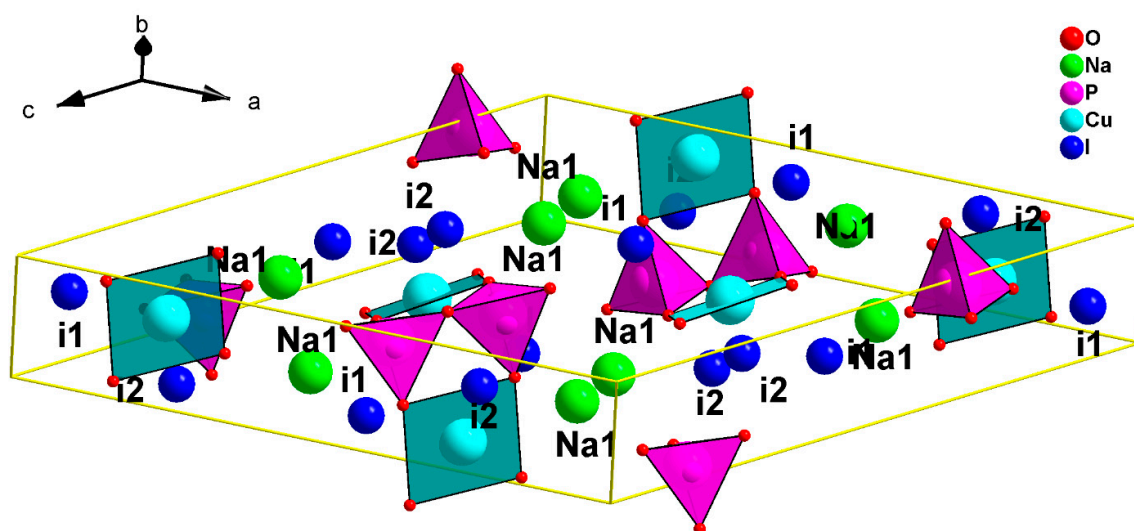


**Figure 11.** Unit cell of the title compound showing the position of the equilibrium site Na1 and the interstitial sites (i1 and i2).

**Table 10.** Local transport pathways in the anionic framework, energetic barrier (eV) and hop distance (Å).

Local Path	Site 1	Saddle	Site 2	Barrier (eV)	Hop Distance (Å)
1	i1	s1	Na1	0.354	1.904
2	Na1	s2	Na1	0.466	3.119
3	i1	s3	i1	0.261	4.145
4	i1	s4	Na1	0.602	2.593
5	i2	s5	i2	0.033	0.955
6	i2	s6	i1	0.582	2.922

Table 10. Cont.

Local Path	Site 1	Saddle	Site 2	Barrier (eV)	Hop Distance (Å)
7	i2	s7	Na1	0.960	3.282
8	i1	s8	Na1	1.260	3.168
9	Na1	s9	i1	1.289	3.168
10	i2	s10	i1	1.355	3.956

Figure 11 shows that the migration along the  $b$  direction does not involve any interstitial sites, and the diffusion occurs from the equilibrium site Na1 to its symmetry image, with a jump distance of approximately 3.119 Å and with an activation energy of approximately 0.466 eV (Figure 12a).

Along the  $c$  direction, Figure 11 shows that the sodium moves from the Na1 position to the interstitial sites i2 then to i1 to reach the equivalent Na1 site (Figure 12b) with an activation energy along this direction of approximately 0.96 eV (Figure 12b).

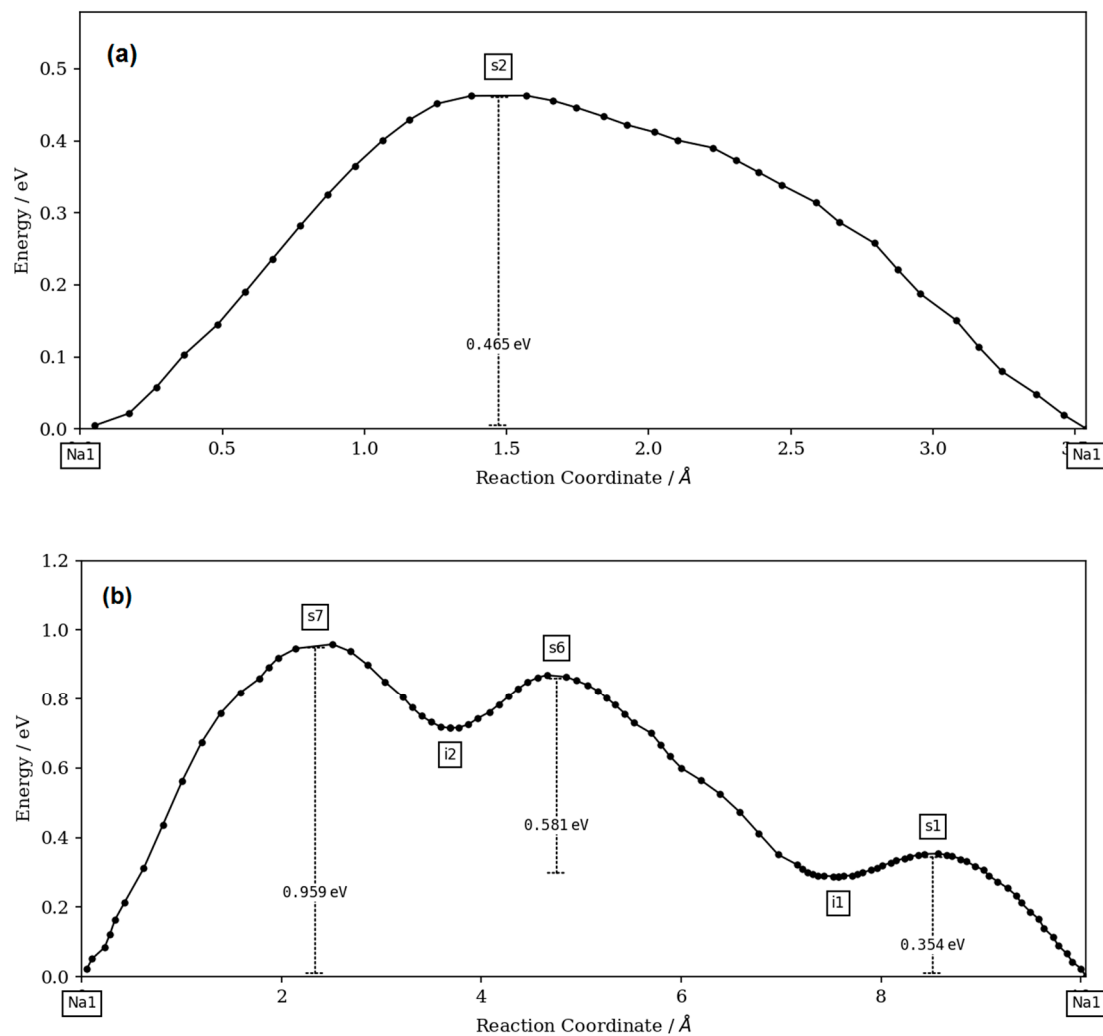
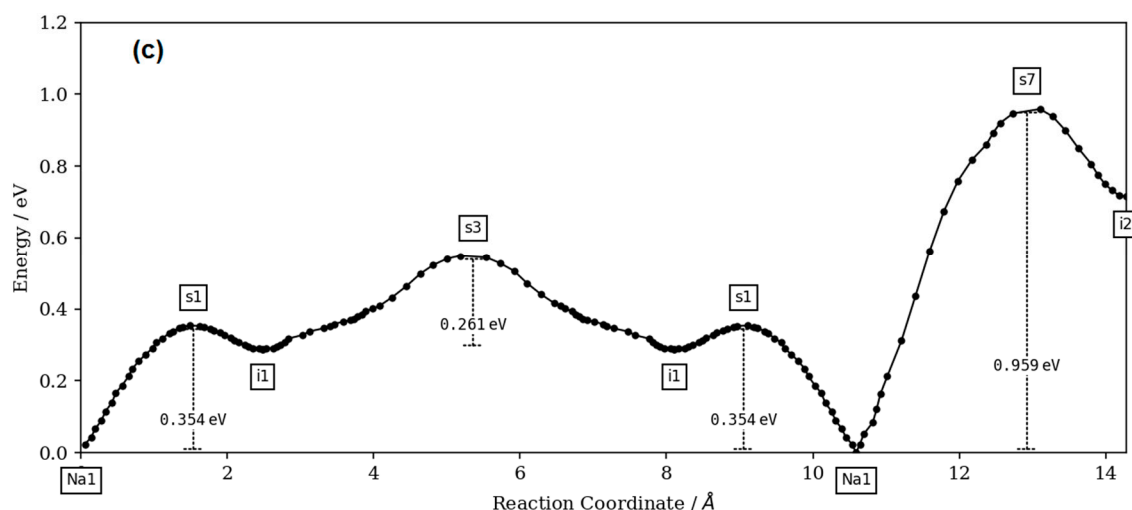
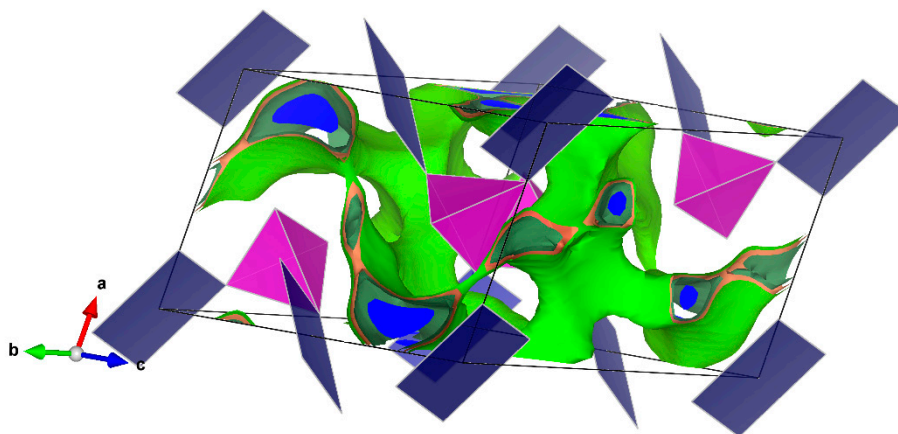


Figure 12. Cont.



**Figure 12.** Variation of energy as a function of the reaction coordinate along the (a) *b*-direction, (b) *c*-direction and (c) *a*-direction.

Along the *a* direction, the sodium atoms pass through the following sites: Na1-i1-i1-Na1-i2. The activation energy along this direction is approximately 0.96 eV (Figure 12c). Thus, the activation energy of the title compound for 1D and 3D ionic conductivity is approximately 0.466 eV and 0.96 eV, respectively. Figure 13 shows the isosurfaces of conduction pathways.



**Figure 13.** Isosurfaces of conduction showing the polyhedral of coordination and the 3D ionic conductivity pathways transport of sodium in  $\text{Na}_2\text{CuP}_{1.5}\text{As}_{0.5}\text{O}_7$ .

Consequently, based on the BVSE calculations, the fast ionic conductivity observed for the material can be explained by the three-dimensional mobility of  $\text{Na}^+$  ions in the inter-ribbon space, likely with more favorable diffusion along the *b*-axis.

#### 4. Conclusions

A new quaternary oxide  $\text{Na}_2\text{CuP}_{1.5}\text{As}_{0.5}\text{O}_7$  was identified in the  $\text{Na}_2\text{O}$ - $\text{CuO}$ - $\text{P}_2\text{O}_5$ - $\text{As}_2\text{O}_5$  system. It crystallizes in the monoclinic  $C2/c$  space group and is isostructural to  $\beta\text{-Na}_2\text{CuP}_2\text{O}_7$ . The partial substitution of P appears to be beneficial for ionic conductivity as the material exhibits lower activation energy of 0.6 eV vs. 0.89 eV for the parent  $\beta\text{-Na}_2\text{CuP}_2\text{O}_7$ . According to the impedance spectroscopy performed on the 88% dense pellet, the bulk ionic conductivity reaches the value of  $2.28 \times 10^{-5} \text{ Scm}^{-1}$ , which allows  $\text{Na}_2\text{CuP}_{1.5}\text{As}_{0.5}\text{O}_7$  to classify as a fast ion conductor. The bond-valence site energy

calculations suggest that the Na<sup>+</sup> diffusion is three-dimensional with some preference for transport along the *b* axis.

**Author Contributions:** Investigation, O.S.A.A., M.M.A. and M.A.; methodology, R.M.; software, Y.B.S.; supervision, R.M. and R.B.T.; validation, M.F.Z.; visualization, M.M.A.; writing—original draft, O.S.A.A. and R.M.; writing—review and editing, Y.B.S., M.A., R.B.T. and M.F.Z. All authors have read and agreed to the published version of the manuscript.

**Funding:** This research was funded by the Deanship of Scientific Research at King Khalid University, grant number R.G.P.1/150/40.

**Acknowledgments:** The authors extend their appreciation to the Deanship of Scientific Research at King Khalid University for funding this work through the research group program under grant number R.G.P.1/150/40.

**Conflicts of Interest:** The authors declare no conflict of interest.

## References

- Nagpure, M.; Shinde, K.N.; Kumar, V.; Ntwaeaborwa, O.M.; Dhoble, S.J.; Swart, H.C. Combustion synthesis and luminescence investigation of Na<sub>3</sub>Al<sub>2</sub>(PO<sub>4</sub>)<sub>3</sub>: RE (RE = Ce<sup>3+</sup>, Eu<sup>3+</sup> and Mn<sup>2+</sup>) phosphor. *J. Alloys Compd.* **2010**, *492*, 384–388. [[CrossRef](#)]
- Chen, J.G.; Ang, L.; Wang, C.; Wei, Y. Sol-Gel Preparation and Electrochemical Properties of Na<sub>3</sub>V<sub>2</sub>(PO<sub>4</sub>)<sub>2</sub>F<sub>3</sub> Composite Cathode Material for Lithium Ion Batteries. *J. Alloys Compd.* **2009**, *478*, 604–607.
- Kanazawa, T. *Inorganic Phosphate Materials, Materials Science Monographs 52*; Elsevier: Amsterdam, The Netherlands, 1989.
- Hong, S.Y.P. Crystal structures and crystal chemistry in the system Na<sub>1+x</sub>Zr<sub>2</sub>Si<sub>x</sub>P<sub>3-x</sub>O<sub>12</sub>. *Mater. Res. Bull.* **1976**, *11*, 173. [[CrossRef](#)]
- Erragh, F.; Boukhari, A.; Elouadi, B.; Holt, E.M. Crystal Structures of Two Allotropic Forms of Na<sub>2</sub>CoP<sub>2</sub>O<sub>7</sub>. *J. Cryst. Spectrosc.* **1991**, *21*, 321–326. [[CrossRef](#)]
- Padhi, A.K.; Nanjundaswamy, K.S.; Goodenough, J.B. Phospho-olivines as Positive-Electrode Materials for Rechargeable Lithium Batteries. *J. Electrochem. Soc.* **1997**, *144*, 1188–1194. [[CrossRef](#)]
- Goodenough, J.B.; Hong, H.Y.-P.; Kafalas, J.A. Fast Na<sup>+</sup>-ion transport in skeleton structures. *Mater. Res. Bull.* **1976**, *11*, 203–220. [[CrossRef](#)]
- Kobashi, D.; Kohara, S.; Yamakawa, J.; Kawahara, A. Un Monophosphate Synthétique de Sodium et de Cobalt: Na<sub>4</sub>Co<sub>7</sub>(PO<sub>4</sub>)<sub>6</sub>. *Acta Cryst.* **1998**, *C54*, 7–9. [[CrossRef](#)]
- Marzouki, R.; Frigui, W.; Guesmi, A.; Zid, M.F.; Driss, A. β-Xenophyllite-type Na<sub>4</sub>Li<sub>0.62</sub>Co<sub>5.67</sub>Al<sub>0.71</sub>(AsO<sub>4</sub>)<sub>6</sub>. *Acta Cryst.* **2013**, *E69*, i65–i66. [[CrossRef](#)]
- Arroyo-de Dompablo, M.E.; Amadora, U.; Alvarez, M.; Gallardo, J.M.; Garcia-Alvarado, F. Novel olivine and spinel LiMAsO<sub>4</sub> (M = 3d-metal) as positive electrode materials in lithium cells. *Solid State Ion.* **2006**, *177*, 2625–2628. [[CrossRef](#)]
- Prabu, S.M.; Selvasekarapandian, M.V.; Reddy, B.V.R. Chowdari. Impedance studies on the 5-V cathode material, LiCoPO<sub>4</sub>. *J. Solid State Electrochem.* **2012**, *16*, 1833–1839. [[CrossRef](#)]
- Reddy, M.V.; Rao, G.V.S.; Chowdari, B.V.R. Metal Oxides and Oxysalts as Anode Materials for Li Ion Batteries. *Chem. Rev.* **2013**, *113*, 5364–5457. [[CrossRef](#)] [[PubMed](#)]
- Sanz, F.; Parada, C.; Rojo, J.M.; Ruiz-Valero, C.; Saez-Puche, R. Studies on Tetragonal Na<sub>2</sub>CoP<sub>2</sub>O<sub>7</sub>, a Novel Ionic Conductor. *J. Solid State Chem.* **1999**, *145*, 604–611. [[CrossRef](#)]
- Chouaib, S.; Ben Rhaiem, A.; Guidara, K. Dielectric relaxation and ionic conductivity studies of Na<sub>2</sub>ZnP<sub>2</sub>O<sub>7</sub>. *Bull. Mater. Sci.* **2011**, *34*, 915–920. [[CrossRef](#)]
- Marzouki, R.; Ben Smida, Y.; Sonni, M.; Avdeev, M.; Zid, M.F. Synthesis, structure, electrical properties and Na<sup>+</sup> migration pathways of Na<sub>2</sub>CoP<sub>1.5</sub>As<sub>0.5</sub>O<sub>7</sub>. *J. Solid State Chem.* **2019**, in press. [[CrossRef](#)]
- Toby, B.J. EXPGUI, a graphical user interface for GSAS. *J. Appl. Crystallogr.* **2001**, *34*, 210–213. [[CrossRef](#)]
- Erragh, F.; Boukhari, A.; Abraham, F.; Elouadi, B. The crystal structure of α- and β-Na<sub>2</sub>CuP<sub>2</sub>O<sub>7</sub>. *J. Solid State Chem.* **1995**, *120*, 23–31. [[CrossRef](#)]
- Nespolo, M.; Guillot, B. CHARDI2015: charge distribution analysis of non-molecular structures. *J. Appl. Cryst.* **2016**, *49*, 317–321. [[CrossRef](#)]
- Adams, S.; Rao, R.P. Transport pathways for mobile ions in disordered solids from the analysis of energy-scaled bond-valence mismatch landscapes. *Phys. Chem. Chem. Phys.* **2009**, *11*, 3210–3216. [[CrossRef](#)]

20. Adams, S.; Rao, R.P. High power lithium ion battery materials by computational design. *Phys. Status Solidi* **2011**, *A208*, 1746–1753. [[CrossRef](#)]
21. Pauling, L. The principles determining the structure of complex ionic crystals. *J. Am. Chem. Soc.* **1929**, *51*, 1010–1026. [[CrossRef](#)]
22. Brown, I.D.; Altermatt, D. Bond-valence parameters obtained from a systematic analysis of the Inorganic Crystal Structure Database. *Acta Cryst.* **1985**, *B41*, 244–247. [[CrossRef](#)]
23. Adams, S. Relationship between bond valence and bond softness of alkali halides and chalcogenides. *Acta Cryst.* **2001**, *B57*, 278–287. [[CrossRef](#)] [[PubMed](#)]
24. Mazza, D. Modeling ionic conductivity in Nasicon structures. *J. Solid State Chem.* **2001**, *156*, 154–160. [[CrossRef](#)]
25. Marzouki, R.; Ben Smida, Y.; Guesmi, A.; Georges, S.; Ali, I.H.; Adams, S.; Zid, M.F. Structural and Electrical Investigation of New Melilite Compound  $K_{0.86}Na_{1.14}CoP_2O_7$ . *Int. J. Electrochem. Sci.* **2018**, *13*, 11648–11662. [[CrossRef](#)]
26. Ben Moussa, M.A.; Marzouki, R.; Brahmia, A.; Georges, S.; Obbade, S.; Zid, M.F. Synthesis and Structure of New Mixed Silver Cobalt (II)/(III) Diphosphate- $Ag_{3.68}Co_2(P_2O_7)_2$ . Silver (I) Transport in the Crystal. *Int. J. Electrochem. Sci.* **2019**, *14*, 1500–1515. [[CrossRef](#)]
27. Chen, H.; Wong, L.L.; Adams, S. SoftBV—a software tool for screening the materials genome of inorganic fast ion conductors. *Acta Cryst.* **2019**, *B75*, 18–33. [[CrossRef](#)]
28. Ben Said, R.; Louati, B.; Guidara, K. Electrical properties and conduction mechanism in the sodium-nickel diphosphate. *Ionics* **2014**, *20*, 703–711. [[CrossRef](#)]
29. Li, H.; Zhang, Z.; Xu, M.; Bao, W.; Lai, Y.; Zhang, K.; Li, J. Triclinic Off-stoichiometric  $Na_{3.12}Mn_{2.44}(P_2O_7)_2/C$  Cathode Materials for High Energy/Power Sodium-ion Batteries. *Appl. Mater. Interfaces* **2018**, *10*, 24564–24572. [[CrossRef](#)]
30. Nakamoto, K. *Infrared and Raman Spectra of Inorganic and Coordination Compounds*, 3rd ed.; Wiley-Inter-Science: New York, NY, USA, 1978.
31. Krichen, M.; Gargouri, M.; Guidara, K.; Megdiche, M. Phase transition and electrical investigation in lithium copper pyrophosphate compound  $Li_2CuP_2O_7$  using impedance spectroscopy. *Ionics* **2017**, *23*, 3309–3322. [[CrossRef](#)]
32. Langlois, S.; Couret, F. Flow-through and flow-by porous electrodes of nickel foam. I. Material characterization. *J. Appl. Electrochem.* **1989**, *19*, 43. [[CrossRef](#)]
33. Hafidi, E.; El Omari, M.; El Omari, M.; Bentayeb, A.; Bennazha, J.; El Maadi, A.; Chehbouni, M. Conductivity studies of some diphosphates with the general formula  $Al_2BIIP_2O_7$  by impedance spectroscopy. *Arab. J. Chem.* **2013**, *6*, 253–263. [[CrossRef](#)]
34. Marzouki, R.; Guesmi, A.; Zid, M.F.; Driss, A. Synthesis, Crystal Structure and Electrical Properties of a New Mixed Compound  $(Na_{0.71}Ag_{0.29})_2CoP_2O_7$ . *Cryst. Struct. Theory Appl.* **2013**, *1*, 68–73. [[CrossRef](#)]
35. Ben Smida, Y.; Marzouki, R.; Guesmi, A.; Georges, S.; Zid, M.F. Synthesis, structural and electrical properties of a new cobalt arsenate  $NaCo_2As_3O_{10}$ . *J. Solid State Chem.* **2015**, *221*, 132–139. [[CrossRef](#)]
36. Marzouki, R.; Guesmi, A.; Zid, M.F.; Driss, A. Etude physico-chimiques du monoarséniate mixte  $Na_4Co_{5.63}Al_{0.91}(AsO_4)_6$  et simulation des chemins de conduction. *Ann. Chim. Sci. Mat.* **2013**, *38*, 117. [[CrossRef](#)]
37. Nasri, R.; Marzouki, R.; Georges, S.; Obbade, S.; Zid, M.F. Synthesis, sintering, electrical properties, and sodium migration pathways of new lyonsite  $Na_2Co_2(MoO_4)_3$ . *Turk. J. Chem.* **2018**, *42*, 1251. [[CrossRef](#)]

